Meteoritics & Planetary Science 39, Nr 12, 1897–1910 (2004)
Abstract available online at http://meteoritics.org

Non-equilibrium concepts lead to a unified explanation of the formation of chondrules and chondrites

Milton BLANDER,[1*] Arthur D. PELTON,[2] In-Ho JUNG,[2] and Richard WEBER[3]

[1]QUEST Research, 1004 East 167th Place, South Holland, Illinois 60473–3114, USA
[2]Ecole Polytechnique, C. P. 6079, Succ. Centre Ville, Montreal, Quebec H3C 3A7, Canada
[3]CRI Containerless Research Incorporated, 910 University Place, Evanston, Illinois 60201–3149, USA
[*]Corresponding author: E-mail: mblander2@aol.com

(Received 7 April 2004; revision accepted 25 September 2004)

Abstract–Calculations of the formation of seven types of chondrules in Semarkona from a gas of solar composition were performed with the FACT computer program to predict the chemistries of oxides (including silicates), developed by the authors and their colleagues. The constrained equilibrium theory was used in the calculations with two nucleation constraints suggested by nucleation theory. The first constraint was the blocking of Fe and other metal gaseous atoms from condensing to form solids or liquids because of very high surface free energies and high surface tensions of the solid and liquid metals, respectively. The second constraint was the blocking of the condensation of solids and the formation of metastable liquid oxides (including silicates) well below their liquidus temperatures. Our laboratory experiments suggested subcooling of type IIA chondrule compositions of 400 degrees or more below the liquidus temperature. The blocking of iron leads to a supersaturation of Fe atoms, so that the partial pressure of Fe (p_{Fe}) is larger than the partial pressure at equilibrium (p_{Fe}(eq)). The supersaturation ratio $S = p_{Fe}/p_{Fe}(eq)$ becomes larger than 1 and increases rapidly with a decrease in temperature. This drives the reaction $Fe + H_2O \Leftrightarrow H_2 + FeO$ to the right. With S = 100, the activity of FeO in the liquid droplet is 100 times as large as the value at equilibrium. The FeO activities are a function of temperature and provide relative average temperatures of the crystallization of chondrules. Our calculations for the LL3.0 chondrite Semarkona and our study of some non-equilibrium effects lead to accurate representations of the compositions of chondrules of types IA, IAB, IB, IIA, IIAB, IIB, and CC. Our concepts readily explain both the variety of FeO concentrations in the different chondrule types and the entire process of chondrule formation. Our theory is unified and could possibly explain the formation of chondrules in all chondritic meteorites as well as provide a simple explanation for the complex chemistries of chondrites, and especially for type 3 chondrites.

INTRODUCTION

This paper is a sequel to the paper entitled "Nucleation constraints lead to molten chondrule precursors in the early solar system" (Blander et al. 2001). The data needed to understand the processes that form solid condensates of ordinary chondrites in the solar system are undoubtedly embedded in the meteorites, with the largest data density being present in unequilibrated (type 3.0) chondrites. These pristine meteorites have apparently accreted at temperatures low enough to preserve the information on the formation of the individual chondrules. In this paper, we focus on data for the Semarkona type LL3.0 chondrite, a sort of Rosetta Stone that will tell us about some of the processes involved in its formation. The non-equilibrium nature of this meteorite leads to far more information than is present in the more equilibrated chondrites (i.e., 3.1–3.6), and all type 3.0 chondrites could contain information that possibly exceeds all the astrophysical information content now available for deducing the origins of the solar system.

Before studying the available data, we must discuss some possible non-equilibrium mechanisms important in the formation of chondrules and chondrites from a solar nebula with a solar composition (Table 1) (Anders and Grevesse 1989). As discussed in the previous paper (Blander et al. 2001), we utilize the constrained equilibrium theory (Blander and Katz 1967; Blander and Abdel-Gawad 1969), in which two well-understood nucleation constraints are imposed in the

Table 1. Nebular gas composition (molar) (Anders and Grevesse 1989).

H	C	O	Si	S	Fe	Na	Ca	Al	Mg	Cr	Mn	Ti
27900	10.1	23.8	1.00	0.515	0.90	0.0574	0.0611	0.0849	1.074	0.0135	0.00955	0.0024

condensation of chondrule precursors in a rain-like process in the nebula, which largely forms metastable liquid silicates.

Two nucleation constraints are considered in the calculation, in the first of which the formation of solid silicates is constrained because of the usually very high surface free energy of solids that, according to nucleation theory, leads to the formation of quite "stable" (long-lived) metastable liquid silicate droplets that have lower surface tensions than the surface free energy of the solids. Our recent experimental studies have shown that metastable silicate liquids can exist at temperatures more than 400 degrees below their liquidus temperatures.

The second nucleation constraint considered is that the formation of solid iron-nickel alloys (which have very large surface tensions for the liquids and surface free energies for the solids) from solar gas is blocked, leading to the supersaturation of iron and nickel atoms in the gas (Blander and Katz 1967). The supersaturation of iron, for example, increases with a decrease in the temperature. Thus, if we consider the equilibrium $Fe + H_2O \Leftrightarrow H_2 + FeO$, where FeO is a component of the liquid droplets, the FeO activity at equilibrium is small in the solar nebula because the reducing conditions are strong at the H_2/H_2O ratio of 586. However, with the supersaturation of iron, the activity of FeO will be larger by a factor equal to the supersaturation ratio of the partial pressure of the supersaturated iron atoms divided by the partial pressure at equilibrium. Therefore, if the supersaturation ratio is 100, the activity of FeO will be 100 times higher than at equilibrium. Since the supersaturation of iron increases with a decrease in temperature, the FeO activities provide us with a relative thermometer, allowing us to calculate the approximate temperatures at which the chondrules crystallized, a transition wherein the solids form and cease to interact with the solar gas.

These major constraints lead to the most important non-equilibrium influences in the formation of chondrules. One of these influences, the increase in the activity and concentration of FeO, provides us with information on the average temperatures of crystallization. The metastable subcooled droplets crystallize by the process of recalescence, in which the released enthalpy of fusion during the crystallization heats up the droplets considerably. The rates of crystallization are driven by the instability and are initially quite rapid for type I chondrules, the first to crystallize, and become slower at lower temperatures up to the cryptocrystalline chondrules, the last to crystallize. The rates of crystallization are relatively rapid in the early stage 1 of recalescence because of the large deviations of the free energy from equilibrium and the sharp release of heat. The rate slows significantly in stage 2 of recalescence, when the temperature has gone somewhat beyond its maximum. The rate is slower yet in stage 3, in which the cooling chondrule asymptotically approaches the original ambient temperature of the molten chondrule precursor.

Early in stage 1, when crystallization is most rapid, the earliest compositions of the crystals are probably diffusionally limited, so the ratio of FeO/MgO in the crystals is close to the original ratio of FeO/MgO in the liquid precursor. A small number of such crystals have been observed in Semarkona by Jones et al. (Jones 1994, 1996a, 1996b). Crystals formed later at slower crystallization rates are likely to be closer to equilibrium. Calculations of the maximum rise in temperature above the ambient temperature in an adiabatic (i.e., no escape of heat) crystallizing droplet at average temperatures of 1500 K show this rise to be approximately 200 degrees. In the real world, the brightening of the droplets leads to radiation losses. For example, if half the heat radiates before the maximum temperature is attained, the maximum increase would be of the order of 100 degrees above the ambient temperature and the ambient temperature, which is the first and last temperature in the initial crystallization, would be roughly 50 degrees below the average temperature during recalescence. The above non-equilibrium effects are related to the constrained equilibrium theory, and are the most important for understanding the chemistry of chondrules.

CALCULATIONS OF AVERAGE CHONDRULE COMPOSITIONS

In this paper, we perform calculations on the chondrule types IA, IAB, IB, IIA, IIAB, IIB, and CC (cryptocrystalline). The FeO content, or more precisely, the FeO activity, of these chondrules increases in the order given, indicating that the crystallization temperatures decrease in the same order. Because of small differences in the average measured compositions of IAB and IB as well as IIAB and IIB, we have substituted the average of these two pairs to simplify the calculations in Table 2. The calculations were performed for a solar gas of 0.1 bar. This pressure was chosen from unpublished calculations for a distance of 1 AU from the sun using a calculational method for solar-type nebulae formation (Bell et al. 1997). This pressure seems to give the believable temperatures we observed in the laboratory (discussed later) for spontaneous fine-grained droplet crystallization. However, as will be shown, the assumption of other pressures in the range from 10^{-3} to 1 bar give analogous results but different crystallization temperatures.

The experimental data in Table 2 were taken from several papers (McCoy et al. 1991; Jones and Scott 1989; Jones 1990;

Table 2. Chondrule compositions (non-metallic phases only).

		Composition (wt%)										Relative	
		SiO_2	MgO	FeO	CaO	Al_2O_3	TiO_2[a]	Cr_2O_3[b]	MnO	Na_2O	FeS[c]	mass	Reference
IA, 1547 K													
Overall	*obs*	*46.9*	*42.6*	*1.24*	*3.66*	*4.09*	*0.20*	*0.46*	*0.13*	*0.54*	*0.20*		[ ]
	calc	42.6	48.0	1.24	3.4	4.3	0.20	0.10	0.017	0.011	0.20	24.8	
Olivine	*obs*	*42.2*	*55.8*	*1.03*	*0.31*	*0.14*	*0.04*	*0.37*	*0.09*				[ ]
	calc	42.4	55.9	1.26	0.39							20.1	
Mesos-tases	*obs*	*52.9*	*5.17*	*0.75*	*16.01*	*21.92*	*0.85*	*0.43*	*0.12*	*1.84*			[ ]
	calc	43.5	14.3	1.17	16.5	22.9	1.04	0.50	0.089	0.06		4.1	
(IAB + IB), 1490 K													
Overall	*obs*	*57.1*	*33.8*	*3.20*	*1.73*	*2.39*	*0.11*	*0.58*	*0.34*	*0.53*	*0.23*		[ ]
	calc	56.9	33.3	3.21	2.71	3.42	0.15	0.19	0.055	0.034	0.12	10.5	
Pyroxene	*obs*	*58.4*	*37.1*	*2.74*	*0.28*	*0.43*	*0.06*	*0.67*	*0.32*				[ ]
	calc	59.0	37.4	2.86	0.82							8.7	
Mesos-tases	*obs*	*61.6*	*3.39*	*3.11*	*7.71*	*18.0*	*0.51*	*0.34*	*0.76*	*4.67*			[ ]
	calc	47.3	14.5	4.85	11.6	19.4	0.87	1.05	0.32	0.19		1.8	
Olivine	*obs*	*42.0*	*52.6*	*4.40*	*0.12*			*0.53*	*0.37*				[ ]
IIA, 1452 K													
Overall	*obs*	*45.5*	*31.6*	*15.1*	*1.91*	*2.70*	*0.10*	*0.51*	*0.39*	*1.66*	*0.95*		[ ]
	calc	44.8	32.7	15.3	2.7	3.4	0.15	0.62	0.18	0.18	0.16	43.9	
Olivine	*obs*	*39.6*	*44.6*	*14.9*	*0.13*			*0.43*	*0.34*				[ ]
	calc	39.5	43.2	17.2	0.13							31.5	
Mesos-tases	*obs*	*62.0*	*7.13*	*8.61*	*7.89*	*9.63*	*0.41*	*0.47*	*0.32*	*3.45*			[ ]
	calc	58.2	6.0	10.5	9.3	12.2	0.55	2.2	0.64	0.63		12.4	
(IIAB + IIB), 1451 K													
Overall	*obs*	*54.8*	*26.7*	*10.2*	*2.17*	*3.53*	*0.13*	*0.53*	*0.46*	*1.33*	*0.13*		[ ]
	calc	51.8	30.2	11.2	2.6	3.2	0.15	0.62	0.15	0.11	0.12	19.0	
Pyroxene	*obs*	*56.9*	*32.0*	*9.50*	*0.28*	*0.20*	*0.03*	*0.67*	*0.41*				[ ]
	calc	57.1	32.0	10.0	0.85							10.2	
Olivine	*obs*	*39.8*	*43.9*	*15.1*	*0.11*			*0.50*	*0.53*				[ ]
	calc	39.9	45.3	14.6	0.15							4.9	
Mesos-tases	*obs*	*64.8*	*1.46*	*10.4*	*4.65*	*13.4*	*0.47*	*0.12*	*0.44*	*4.25*			[ ]
	calc	52.9	6.5	10.1	10.1	15.8	0.70	3.05	0.74	0.53		3.9	
Cryptocrystalline, 1435 K													
Overall	*obs*	*52.0*	*24.1*	*19.0*		*1.73*	*0.09*	*0.63*	*0.75*				[ ]
	calc	55.8	21.4	18.6	1.4	1.8	0.08	0.65	0.16	0.11	0.18	1.8	
Pyroxene	calc	54.6	25.1	19.8	0.50							1.5	
Mesos-tases	calc	62.1	3.4	12.5	5.9	10.6	0.5	3.9	0.91	0.62		0.3	

[a]Calculated (Ti_2O_3 + TiO_2) reported as "TiO_2."
[b]Calculated (CrO + Cr_2O_3) reported as "Cr_2O_3."
[c]S reported as "FeS."
Metallic Fe-Ni and minor constituents are not included in the observed compositions, which have been renormalized to 100%.

1994, 1996a, 1996b; Grossman et al. 2000). Type IA chondrules contain only or mainly low-FeO olivine as the crystal phase. Small amounts of pyroxene may also be present. The IAB chondrules contain both low-FeO olivine and more abundant pyroxene in various ratios, while the IB chondrules contain only or mainly pyroxene. There are no sharp demarcations between these classifications. Type II chondrules are similar, but the FeO content is higher, with IIA containing only or mainly high-FeO olivine as the crystalline phase, with some pyroxene in most. Types IIAB and IIB contain both FeO-rich olivine and pyroxene in different ratios which indicate that the average is largely pyroxene, while the cryptocrystalline (CC) chondrules probably contain mainly pyroxene and some glass. For all reported "observed" compositions shown in Table 2, the contents of minor constituents, such as K_2O and P_2O_5, were not included. The metallic Fe/Ni phase, generally reported to account for 1–8% of the total mass, was not included; the compositions shown in Table 2 were renormalized to sum to 100%.

Supersaturation of iron is present at all temperatures of the chondrules we considered, since the activities of FeO in the calculation and in the measurements of the chondrule compositions increase in going from Type IA to CC chondrules. The measurements of growing FeO content at lower temperatures supports this blockage of iron. However, a relatively small amount of metals, Fe-Ni alloys, and calcium-aluminum-rich inclusion (CAI) nuggets are inside the chondrules and CAIs. But how can there be metal if most metals are blocked? This can be explained by the fact that nucleation is a stochastic process, meaning that there is a small probability of a modest amount of metal forming spontaneously. This probability is increased with an increase of supersaturation. Consequently, some small amount of metal will precipitate especially at high supersaturation. If these droplets remained in the gas for a long time, they would grow to fairly large sizes (e.g., a good fraction of chondrule sizes). The droplets remain small because they readily enter the molten chondrules, where they can be seen inside. Some Fe-Ni alloys appear to have condensed on chondrules after crystallization, probably when most of the chondrules are crystallized. The best examples are the armored chondrules. What forces the small metal droplets into the liquid chondrules? The answer is related to surface tensions (for liquids) or surface free energies (for solids).

Liquid silicates have fairly large surface tension (in the hundreds of ergs/cm^2). Molten or solid iron have larger surface tension values (1800 erg/cm^2), and these values are even larger for the solid iron. When condensed solid or liquid metal touches liquid silicates, the interfacial tension between metal and silicates is smaller than that of the sum of the surface tensions or surface free energies of the metal and silicates. In thermodynamic terms, the chemical potential of all the surfaces decrease linearly by the area sizes of the interfacial metal and silicate This can be understood if one realizes that silicates have many ionically charged atoms at the interface, some with positive charges and some with negative charges, and that the electrical field in the silicate near the interface creates an opposite charge near the metal surface, which mirrors the one in the silicate. This powerful coulombic interaction lowers the chemical potential of the metal-silica interfacial surface and the chemical potential decreases linearly with the area of the interface. Diffusion is driven by gradients of the chemical potential by the equation (Blander 1953):

$$J = -M\nabla\mu \qquad (1)$$

where J is flow, M is mobility, and $\nabla\mu$ is the gradient of the chemical potential. Thus, because the motional force by the powerful coulombic energies pulls or sucks the metal into the molten chondrules with a growing interface and a lowering of the interfacial chemical potential. This means that the thermodynamic stability of the metal and liquid chondrule has increased by this process. A similar concept is valid for the entrance of nuggets into liquid CAIs. As long as there is a significant number of liquid droplets, metals will readily enter chondrules and CAIs. When most chondrules or CAIs are crystallized and few molten silicates are left, the small amount of nucleated metals will be able to form metals, if available, on the surface of the chondrules and possibly also for the CAIs.

The observed average overall compositions of the phases in several chondrule types listed above are shown in Table 2. We left out several relatively minor chondrule types (e.g., excentroradial, barred olivine, granular) because of a lack of adequate data of these types. Some of these types are either similar to or are an average of some of the types that we considered. Our aim is to relate our calculations of the compositions of condensates to the measured compositions to lend credence to the constrained equilibrium theory, and ultimately to other non-equilibrium effects.

PRIMARY ASSUMPTIONS OF THE MODEL

The primary assumption of the chondrule formation model is that a very large number of metastable liquid silicate droplets formed not very far from the center of the solar nebula (possibly about 1 AU for Semarkona). These droplets in a cooling nebula can cool far below their liquidus temperatures, and fractions of them will nucleate at different times and temperatures. Nucleation can be initiated by an energetic event (e.g., shock waves) or in a turbulent gas by small loose crystals formed as a result of collisions of materials that crystallized earlier (such as CAIs and chondrules). As discussed earlier, when nucleation occurs, subcooled droplets crystallize rapidly (within seconds for type IA and within some minutes for cryptocrystalline droplets) by recalescence. After crystallization, further reaction of the solids with the nebula nearly ceases. However, a small amount of residual liquids, which are precursors of mesostases, can continue to react if exposed to the nebula. We believe that, as the environment cools, these liquids will pick up volatiles, such as sodium and potassium, for example, to enrich the mesostases in these elements at temperatures below the average temperatures of crystallization.

In the present model, we propose that all types of chondrules were formed by this same process of crystallization of supercooled liquid droplets. The different compositions of the different types of chondrules result simply from the different temperatures at which nucleation and crystallization occurred. Nucleation at different temperatures leads to different FeO activities and different overall compositions in each temperature range for the different classes of chondrules. We aim to show that when we calculate the activity of FeO, which indicates the average temperatures of crystallization, the compositions of the other components in the chondrules and the major minerals are essentially the same as is measured. This agreement can be

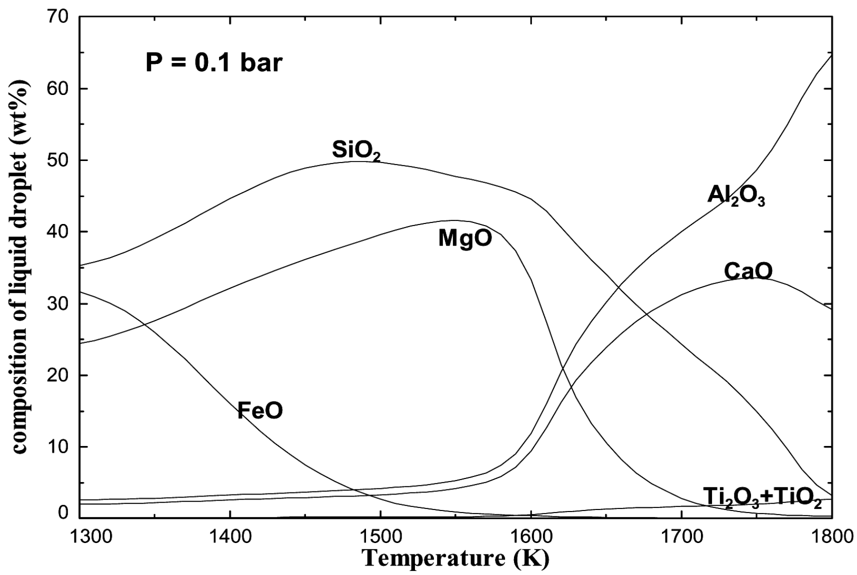

Fig. 1. Composition of droplets in equilibrium with the initial nebula (p = 0.1 bar).

improved even further if we take into account the generally modest non-equilibrium effects (see Appendix) and the relatively small uncertainties of the measurements and calculations. The largest difference between the measured and calculated compositions is in the mesostases. The mass of the mesostases is a small fraction of the total mass of the chondrules. This leads to a large multiple in the wt% of the transfer from the chondrule to the mesostases of components involved in the non-equilibrium effects discussed in the Appendix. The observed compositions of the mesostases are very sensitive to small changes in the chondrule parameters.

Figure 1 shows the thermodynamically calculated composition of condensed supercooled liquid oxide droplets in equilibrium with a solar nebula of the composition given in Table 1 when the total pressure of the nebula is 0.1 bar. At the highest temperatures, the droplets consist of the least volatile oxides, Al_2O_3 and CaO. Crystallization of such droplets at these temperatures would result in the formation of high CaO and Al_2O_3 CAI "chondrules" which are observed in several chondrites, but not in Semarkona. The equilibrium content of the volatile component FeO rises rapidly as the temperature decreases. The FeO content of the chondrules is thus a sensitive indicator of the temperature at which they crystallized. The IA chondrules with the lowest FeO content (about 1.24 wt%) crystallized at the highest temperature, while the cryptocrystalline chondrules with the highest FeO content (about 19%) crystallized at the lowest temperatures. At a temperature of 1533 K and a pressure of 0.1 bar, the exact calculated composition of a supercooled liquid oxide droplet in thermodynamic equilibrium with the nebula is shown in Table 3. Comparison with the overall observed composition of the IA chondrules (first row of Table 2) shows a remarkable agreement for every component, with the sole exception of Na_2O. At 1405 K and at the same pressure of 0.1 bar, the calculated droplet composition in Table 3 is similarly in remarkable agreement with the observed overall compositions of the IIA chondrules, as shown in Table 2.

In Fig. 2, the calculations were repeated for an assumed pressure of 0.001 bar. Figures 1 and 2 can be seen to be nearly identical, except for an average shift of the temperature axis of about 200 degrees. For example, at a pressure of 0.001 bar, equilibrium IA and IIA droplet compositions very close to those shown in Table 3 can be calculated for temperatures of 1334 K and 1231 K. Figure 3 shows the calculated temperature-pressure loci with equilibrium FeO contents equal to 1.24 and 15.1%, which are the observed average FeO contents of IA and IIA chondrules in Table 2. Figures 4 and 5 show the calculated droplet composition as a function of pressure and temperature for an FeO content of 1.24 wt% (type IA). The best agreement between the calculated and observed composition is obtained when the pressure is approximately 0.1 bar, particularly in regard to the FeS content. Furthermore, the assumption of pressures much below 0.1 bar requires the postulation of very large degrees of supercooling. Thus, we chose this pressure for our subsequent calculations. Within the error limits of the observations, however, any assumed pressure (and corresponding temperature from Fig. 3) between approximately 0.001 and 10 bar will give good agreement between calculations and observations. However, the last chondrite type to crystallize, CC chondrules, are likely to crystallize in a temperature range of 1400–1450 K. This temperature was estimated from laboratory measurements. In later studies, we plan to conduct experiments on CC droplets that crystallize spontaneously. The measurements will help determine the real pressure in a nebula, which we now believe is close to 0.1 bar.

The calculated equilibrium liquidus temperatures of oxide droplets of the overall compositions in Table 2 vary

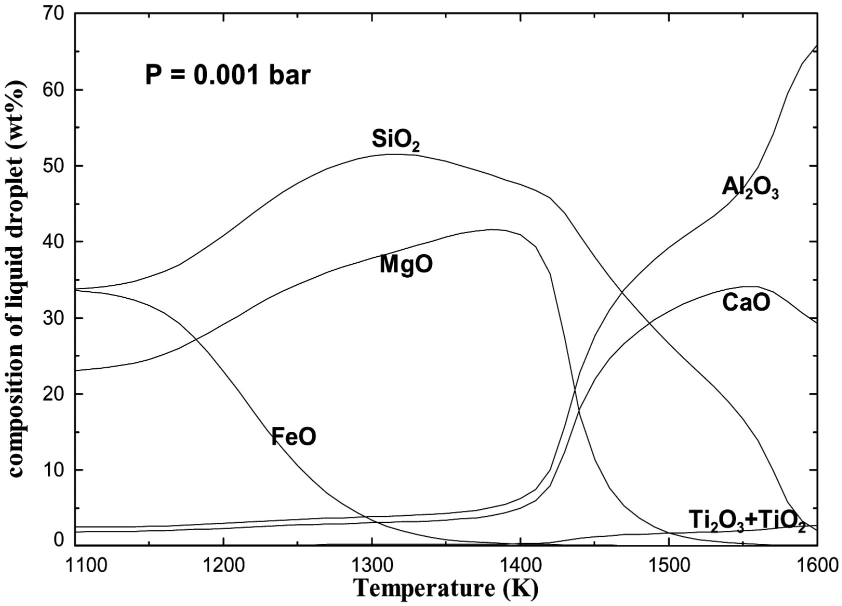

Fig. 2. Composition of droplets in equilibrium with the initial nebula (p = 0.001 bar).

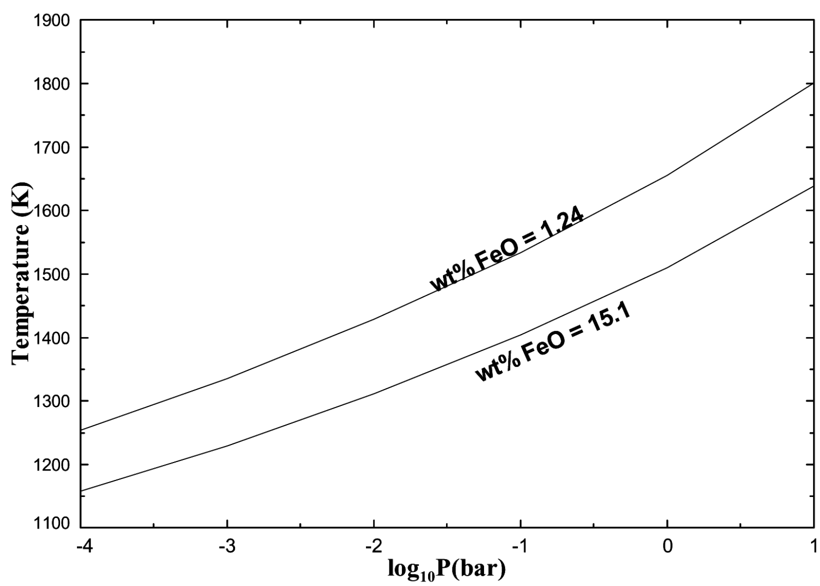

Fig. 3. Temperature-pressure loci for droplets in equilibrium with the initial nebula when the weight % FeO in the droplets are 1.24 and 15.1.

Table 3. Calculated compositions of supercooled liquid precursor droplets in equilibrium with the initial nebula.

T (K)	p (bar)	Composition (wt%) SiO_2	MgO	FeO	CaO	Al_2O_3	TiO_2[a]	Cr_2O_3[b]	MnO	Na_2O	FeS[c]
1533	0.1	48.3	41.1	1.22	3.7	4.7	0.21	0.56	0.06	0.008	0.18
1405	0.1	45.2	32.6	14.8	2.6	3.3	0.13	0.73	0.34	0.04	0.45

[a]Calculated (Ti_2O_3 + TiO_2) reported as "TiO_2."
[b]Calculated (CrO + Cr_2O_3) reported as "Cr_2O_3."
[c]S reported as "FeS."

from approximately 1800 to 2000 K. Hence, undercooling with respect to oxide crystallization of several hundred degrees is postulated. This is not unreasonable, as Blander and Weber (unpublished data) observed supercooling of at least 400 degrees in the laboratory. Furthermore, the model supposes that the nucleation of either solid or liquid metallic

Fe is blocked, though not completely. This constraint has been observed experimentally (Frurip and Bauer 1977).

THE FACT THERMODYNAMIC COMPUTER DATABASES

All thermodynamic calculations have been performed with the FACT thermodynamic computer system, of which Pelton is a principal developer (Pelton et al. 2003). FACT consists of large, multicomponent solution, evaluated databases of the thermodynamic properties of thousands of compounds and solutions, data on over 5000 pure substances, and a suite of programs that use these data to perform chemical equilibrium calculations by means of a general Gibbs energy minimization algorithm (Eriksson 1975). One of the most important features of FACT is that which gives the thermodynamic properties (chemical potentials) as functions of temperature and composition for liquid and solid solutions of oxides (including silicates), salts, sulfides, metals, and so on.

These solution databases have been prepared by first developing an appropriate mathematical model, based upon the structure of the solution, giving the thermodynamic properties as functions of composition and temperature. Next, all available thermodynamic and phase diagram data from the literature are simultaneously "optimized" to obtain one set of critically evaluated self-consistent parameters of the model for all phases in 2-component, 3-component, and, if available, higher-order sub-systems. Finally, the models are used to estimate the thermodynamic properties of an N-component solution from the database of parameters for lower-order sub-systems.

For molten oxide solutions, we used the modified quasi chemical model for short-range ordering, which was developed by the present authors (Blander and Pelton 1983, 1984, 1987; Pelton and Blander 1984, 1986; Pelton and Chartrand 2001), as was the model used to calculate the solubility of sulfur as sulfide ions in the molten silicate solution (Reddy and Blander 1987, 1989; Pelton et al. 1993; Pelton 1999). The olivine and pyroxene solutions are described using a model (Degterov et al. 2001) based on the compound energy formalism (Hillert et al. 1988), which correctly takes account of the distribution of the cations among the various sites in the crystal structure. Other ceramic solid solutions, such as spinels as melilites, are modeled similarly. A database for molten and solid phases in the Fe-Ni-Co-Cr-S system has been developed using the modified quasi chemical model, which is applicable for all compositions from pure metal to pure sulfide.

All data of all types (phase diagrams as functions of T, composition and oxygen potential, activity measurements, calorimetric data, cation distribution data, etc.) from hundreds of original references have simultaneously been taken into account in developing the optimized FACT databases for oxide systems over the past 25 years (Eriksson and Pelton 1993; Eriksson et al. 1993a, 1993b, 1994; Wu et al. 1993a, 1993b; Degterov and Pelton 1996a, 1996b, 1997; Chartrand and Pelton 1999; Degterov et al. 2001, 2002). With the present databases in particular, all available data of all types are reproduced within experimental error limits for the SiO_2-MgO-FeO-Fe_2O_3-CaO-Al_2O_3-(TiO_2-Ti_2O_3-CrO-Cr_2O_3-MnO-Na_2O-S) system, where the components in parentheses are minor constituents. Furthermore, the models permit good estimations to be made in ranges of temperature, composition, and oxygen potential where data have not been measured. Many more components, such as CoO, B_2O_3, ZnO, and PbO, are included in the FACT databases for oxides. Those listed here are only those relevant to the present article.

For the gas phase (solar nebula), ideal gas behavior has been assumed with data taken from the FACT databases for over 150 possible gaseous species, such as H_2, H_2O, CO, Fe, H, H_2S, SiO, Na, Mg, SiS, Mn, HS, Cr, CO_2, CH_4, FeS, and AlOH, for example.

ASSUMPTIONS OF THE DETAILED MODEL

From the above calculations, it can be seen that excellent agreement with the observed compositions of IA and IIA chondrules can be obtained simply by assuming that the composition of a supercooled droplet is the same as the overall composition of the resulting chondrule after crystallization. That is, that the composition does not change during crystallization due to blocking of the exchange of matter with the nebula because of rapid crystallization. On the other hand, in the case of the (IAB + IB), (IIAB + IIB), and cryptocrystalline chondrules, agreement under this assumption was found to be less satisfactory. At temperatures of crystallization chosen to reproduce the observed FeO contents of these chondrules, the calculated SiO_2 contents of the droplets are approximately 10 wt% less than the observed ones. However, in reality, it is expected that exchange of matter with the nebula will occur during crystallization. Although the crystallization process—mostly pyroxene in the case of AB and B type chondrules—occurs over a period of many seconds to a few minutes, this slower crystallization would not be rapid enough to prevent gas/liquid exchange from occurring at these high temperatures. In this regard, it is important to note that the temperature of the droplets will temporarily rise significantly during crystallization by recalescence because of the release of the heat of crystallization. As discussed earlier, calculations indicate a maximum temperature rise of approximately 100 degrees. The temporarily higher temperature makes it even more likely that gas/liquid equilibrium is achieved during crystallization. As the crystallization nears completion, the temperature decreases again and the remaining liquid phase progressively decreases in volume, becomes entrapped between the crystalline grains where it is no longer in contact with the gas,

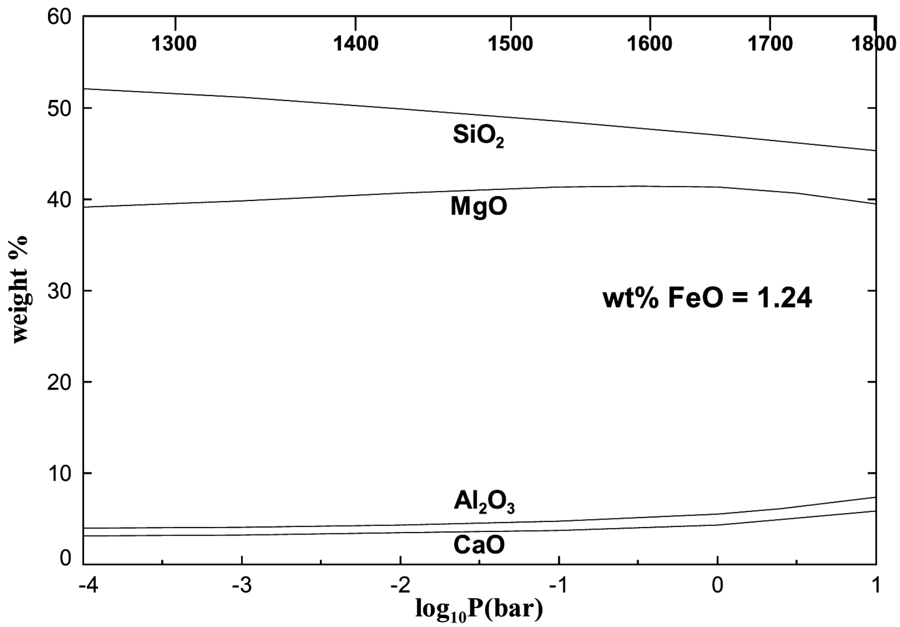

Fig. 4. Droplet compositions of major components in equilibrium with the initial nebula when droplets contain 1.24 wt% FeO.

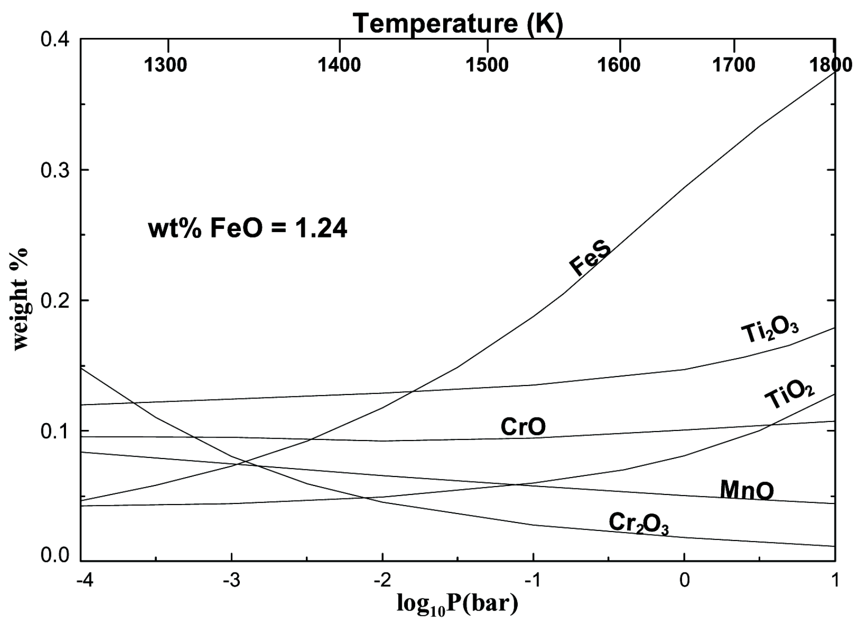

Fig. 5. Droplet compositions of minor components in equilibrium with the initial nebula when droplets contain 1.24 wt% FeO.

and becomes richer in SiO_2, and thus more viscous. All these factors tend to mitigate against gas/liquid equilibrium during the later stages of crystallization. However, even after the temperature of the chondrule has fallen back to its initial value, some small amount of transfer between the nebula and the mesostases could continue. The actual situation is complex. In the present calculations, we have made the simplifying assumptions that the droplets crystallize in complete thermodynamic equilibrium with the surrounding gas until their temperature has returned back to its initial value, and that thereafter, no further exchange with the gas phase occurs. One exception to this rule, discussed later, is made in the case of sulfur.

When this assumption is made, more satisfactory agreement is obtained with the observed compositions of the (IAB + IB), (IIAB + IIB), and cryptocrystalline chondrules, because these chondrules crystallize to yield only or mainly pyroxene. Since pyroxene is a relatively SiO_2-rich and MgO-poor phase, exchange of these constituents occurs with the gas phase during crystallization in order to maintain equilibrium, thereby resulting in a final overall chondrule composition that is richer in SiO_2 and poorer in MgO than the original droplet.

Finally, in order to propose a detailed model, we must address the question of whether the temperature gradient is spatial or temporal. In the former case, we would assume that the droplets all crystallize at approximately the same time but at different locations in a temperature gradient, which could be radial outwards from the sun or perpendicular to the plane of the nebular disk. In the latter case, we would assume that the droplets precipitate progressively with time as the nebula cools, possibly due to adiabatic expansion away from the sun. Although both assumptions yield similar results, the latter was found to give somewhat better agreement with the observed chondrule compositions.

In our present detailed model, therefore, we assume that the droplets and the nebula form a closed isothermal and isobaric system that is gradually decreasing in temperature. The assumption of a closed system means that the composition of the nebula changes slightly as more and more chondrules precipitate. Again, this assumption is not essential, but has been found to give somewhat better agreement between calculations and observations. For the sake of simplicity, the pressure is assumed to be constant at 0.1 bar. Although the expansion and resultant decreasing temperature would be accompanied by a decrease in pressure, this decrease should be relatively small. In any case, as shown earlier, very similar results are obtained over a wide range of pressures. Hence, a decrease in pressure accompanying the decrease in temperature could be accommodated in the model by simply lowering the assumed temperatures of the later crystallization events with little effect on the calculated chondrule compositions. The supercooled liquid droplets are assumed to always be at equilibrium with the nebula. Nucleation of solid or liquid Fe is always constrained.

DETAILED CALCULATIONS

The calculated compositions of non-metallic phases are presented in Table 2, where comparison can be made with measurements made by many authors (e.g., Jones; Grossman) of the average compositions of the different types of chondrules we consider. The calculations are reasonably paired with the observed averages and strongly support the constrained equilibrium theory in general. We have discussed earlier, and will discuss further in the Appendix, the possible non-equilibrium effects that can further decrease the relatively small differences between the measured and calculated compositions down to the uncertainties in the measurements and in the calculations to provide stronger support for the constrained equilibrium theory.

Thirty percent of the droplets present at 1547 K are first assumed to crystallize at this temperature, in equilibrium with the nebula. The resultant calculated overall chondrule composition and the compositions of the olivine and mesostases are shown in Table 2. Agreement with the observations for all components except Na_2O is excellent for the overall composition and the composition of olivine. The calculated composition of the mesostases is lower in SiO_2 and higher in MgO than the observed values. However, this can be understood by the non-equilibrium hypothesis of olivine overgrowth as described in the Appendix. The temperature of 1547 K was chosen in order to reproduce the measured total FeO content of type IA chondrules under the assumption that equilibrium is maintained with the gas phase during crystallization. This temperature differs slightly from the temperature of 1533 K (Table 3), the temperature at which the precursor droplets have this FeO content.

The rapidly crystallized IA chondrules are subsequently assumed to no longer exchange matter with the nebula. The nebula and remaining droplets are then cooled at equilibrium to 1490 K, where calculations show that they are supersaturated with respect to both olivine and pyroxene. In order to simulate the overall composition of type IAB-IB chondrules, we assume that pyroxene nucleates before olivine. This was done to get an approximate value of pyroxene compositions. At this point, uncertainties as to the relative number of IA chondrules which crystallize and the relatively small uncertainties in the computer program to alter the mineral forms. We plan a long series of calculations to determine these uncertainties. Fourteen percent of the remaining droplets present at 1490 K are assumed to crystallize rapidly at this temperature, with only pyroxene and the liquid assumed at equilibrium with the nebula. The resultant calculated overall composition and the compositions of the pyroxene and mesostases are shown in Table 2. Agreement of the overall composition and the pyroxene composition with the observations is remarkable, except, again, for Na_2O. As in the case of the IA chondrules, the calculated composition of the mesostases is lower in SiO_2 and higher in MgO than the observed values (see Appendix).

The decision to permit 30% and 14% of the droplets to crystallize at each of the two temperatures was made arbitrarily. However, the sum of these two percentages was chosen so that the total calculated mass of all type I chondrules would be (24.8 + 10.5)% of the total mass of all the chondrules (Table 2). This is close to the value of roughly 33%, which we have deduced by combining the reported observations (Gooding and Keil 1980; Jones 1994).

Of course, we are not proposing that isolated nucleation events actually occurred at 1547 and 1490 K. As discussed earlier, the compositions of type I chondrules vary continuously from type IA through type IAB to type IB. The observed compositions in Table 2 are averages of groups of chondrules. In reality, the type I chondrules will crystallize stochastically at all temperatures over a range from somewhat above 1547 K to somewhat below 1490 K. As the temperature decreases, the calculations show that the chemical potential of pyroxene relative to that of olivine steadily increases, thereby resulting in the observed tendency for the relative amounts of pyroxene and olivine to vary continuously. This can be understood simply as the result of the fact that the Gibbs energy of the following reaction becomes more negative as temperature decreases:

$$(Mg_2SiO_4(\text{olivine}) + SiO_2 \Leftrightarrow 2MgSiO_3 \tag{2}$$

where the SiO_2 is dissolved in the liquid silicate, which becomes the mesostases. This results in pyroxene becoming relatively more stable than olivine as temperature decreases. Therefore, the calculated IA chondrule composition in Table 2 actually represents the average composition of chondrules that crystallized over a range of temperature around 1547 K and similarly for the chondrules that were calculated to crystallize around 1490 K. The same comment applies, of course, to the crystallization of the type II and cryptocrystalline chondrules discussed later.

As the temperature decreases further still, the chemical potential of olivine again rises relative to that of pyroxene. This is because the higher FeO contents at lower temperatures favor the formation of olivine, as FeO is much more soluble in olivine than in pyroxene. We now continue the process of cooling and crystallization. The (IAB + IB) chondrules are assumed to no longer exchange matter with the nebula, the temperature is reduced to 1452 K, and 70% of the remaining droplets present at 1452 K are assumed to solidify in equilibrium with the nebula at this temperature. This results in a calculated overall composition of IIA chondrules very close to that shown in Table 2, with about 70% olivine and 30% pyroxene as crystalline constituents. However, in order to model the formation of a pure type IIA chondrule, we repeated the calculation with the assumption that only olivine nucleates. This gave the calculated results shown in Table 2 for type IIA chondrules. Agreement with the observations is excellent for all phases, including in this case the mesostases, since olivine overgrowth was essentially assumed as discussed in the Appendix. Note that the assumed temperature of 1452 K differs from the temperature of 1405 K (Table 3), the temperature at which droplets in a nebula in which no solidification has occurred have this level of FeO content. As the temperature decreases further, the relative chemical potential of pyroxene rises again. Furthermore, the previous crystallization of the IIA chondrules, which are rich in olivine, has caused an increase in the SiO_2 content and a decrease in the MgO content of the nebula, thus also favoring the precipitation of pyroxene. Therefore, as the temperature decreases further, pyroxene is progressively favored relative to olivine, thereby resulting in the formation of IAB, IIB, and cryptocrystalline chondrules with progressively higher pyroxene/olivine ratios.

We assume another crystallization event at 1451 K with 95% of the remaining droplets at this temperature crystallizing in equilibrium with the nebula. The calculated results for these (IIAB +IIB) chondrules are shown in Table 2. Agreement with observations is excellent. As with most other chondrules, the observed composition of the mesostases is richer in SiO_2 than the calculated values.

As with type I chondrules, the choice of the percentages of droplets crystallizing at 1452 and 1451 K was arbitrary. However, their sum was chosen so that the total calculated mass of all type II chondrules would be (43.9 + 19)% (Table 1) of the total mass of all chondrules, which is close to the value of roughly 65% deduced from observations (Gooding and Keil 1980; Jones 1994).

Finally, all remaining droplets are assumed to crystallize at 1435 K, giving the calculated overall "cryptocrystalline" composition shown in Table 2, which is in good agreement with the observations. Observations on only two CC chondrules (Grossman et al. 2000) were used to give the average observed composition in Table 2. Because of this, the uncertainties are relatively large. The calculated relative mass of these chondrules (1.8%) is also in agreement with the observations (approximately 2%). For all chondrules, the calculated relative mass of the mesostases varies from approximately 17% to 28% of the total mass (Table 2), which may be compared to the observed ratio reported by Jones of, very roughly, 20%. The results in Table 2 are important as proof of the significance of the constrained equilibrium theory. Further work with other meteorites will strengthen the importance of this theory in meteoritics.

SULFIDE PHASE

As seen in Table 3, the sulfide content of the initial droplets before crystallization is very close to the observed values. Calculations show that all the sulfur is dissolved in the liquid. A separate sulfide-rich phase does not form thermodynamically; however, as crystallization of the olivine and/or pyroxene occurs, the sulfur content of the remaining liquid oxide rapidly increases beyond the saturation limit, and a liquid FeS phase precipitates. The calculations show that nearly all the sulfur in the droplet eventually precipitates as FeS. However, if equilibrium with the gas is presumed to occur during crystallization, then much of the sulfur will be lost to the gas phase during recalescence. Therefore, in order to explain the observed FeS contents of the chondrules, sulfur must be an exception to the assumption of equilibrium with the nebula during crystallization. That is, the liquid FeS phase is assumed to precipitate rapidly enough to prevent appreciable loss of sulfur to the gas. The calculated FeS contents in Table 2 were calculated under this assumption.

Small Fe/Ni particles, which account for approximately 1–8% of the total mass, are observed in most Semarkona chondrules. These may be dust particles in the nebula that have been entrained by the liquid droplets, or they may have resulted from a few Fe/Ni nuclei that have grown slowly within the chondrules. These metallic particles should act as

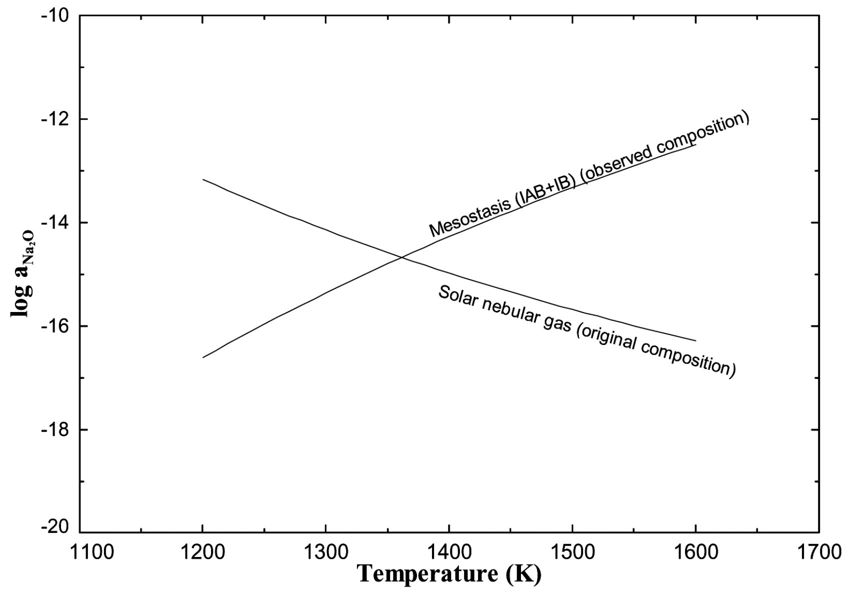

Fig. 6. Activity of Na_2O (with respect to pure liquid standard state) in the initial nebula at p = 0.1 bar and in a liquid phase of the observed compositions of (IAB + IB) mesostases from Table 2.

preferential nucleation sites for the liquid FeS phase, and many of the Fe/Ni particles are in fact surrounded by a sulfide phase. The rest of the sulfur is found as FeS particles. The existence of such nucleation sites could help explain the proposed rapid precipitation of the FeS phase during crystallization. Furthermore, Fe is soluble in liquid FeS. Our calculations show a solubility of approximately 30 mole% Fe in FeS at these temperatures. This dissolution lowers the chemical activity of FeS and also favors precipitation.

A calculation was made to see whether the presence of Fe particles in the original precursor droplets would cause formation of an equilibrium liquid FeS-Fe phase. This does not occur. That is, even in the presence of Fe particles, the original droplets do not contain an equilibrium FeS-rich phase. Saturation is only surpassed during crystallization.

Na_2O CONTENT

As shown in Tables 2 and 3, the calculated Na_2O content of neither the initial droplets nor the crystallized chondrules is as high as the observed concentrations. Virtually all the Na_2O is observed to be in the mesostases as expected. The observed SiO_2 content of the mesostases is generally higher than that calculated. At higher SiO_2 contents, the activity coefficient of Na_2O is lower, thereby favoring dissolution of Na_2O. This, however, can only partially account for the discrepancy, as can be seen in Fig. 6. In this figure, the calculated Na_2O activity, with respect to pure liquid Na_2O as standard state, of a liquid mesostases phase of the observed composition in (IAB + IB) chondrules (Table 2) is plotted versus temperature along with the activity of Na_2O in the nebula. At the supposed crystallization temperature (Table 2) of these chondrules, the activity of the gas is much lower than in the mesostases. However, it can be seen from Fig. 6 that the activities in the two phases rapidly approach each other, becoming equal near 1360 K. That is, the calculated Na_2O content is quite sensitive to relatively small changes in temperature and total pressure. Very similar results are also obtained for the compositions of the mesostases of the other types of chondrules. Sodium is known to be relatively very mobile in molten oxides. We have assumed in the model that, in general, no further exchange occurs between the gas and the solid crystals once crystallization is complete. However, since the mesostases is originally a liquid, it can continue to pick up sodium in the liquids at relatively high temperatures (above the glass transition).

LEVITATION EXPERIMENTS

Containerless processing experiments were carried out to access deeply subcooled liquid in conditions that avoided container-derived sources of nucleation. The compositions of the synthetic powders investigated are those of types IA and IIA, and were prepared by Roger Hewins and his staff. Spherical samples approximately 3 mm in diameter were made by melting powdered crystalline precursor material using a hearth melter. Weighed samples were levitated in a conical nozzle levitator using a redox gas mixture. The gas was comprised of 0.979% CO, 8.97% CO_2, and 90.051% Ar by volume to provide a value of $p(O_2)$, which will preserve the FeO content of the samples at temperatures from 1200 to 2000 K. The levitated sample was slowly heated using a partially focused CO_2 laser beam (Photon Sources, Livonia, MI, model V-500). Progress of the levitation experiment was observed with a video camera equipped with a close-up lens, auto-exposure iris, and a spectral filter with a band pass centered around 650 mm. The output of the video camera was displayed on a monitor and recorded for later review. The temperature range for the experiments was 1200 to 2000 K.

The apparent temperature of the sample was measured at a rate of 30 Hz with an automatic optical pyrometer that operated at a wavelength of 650 nm and sampled a spot approximately 1 mm in diameter on the surface of the sample. Temperature data were recorded by computer. Apparent temperatures measured with the pyrometer were corrected using the estimated spectral emissivity of the sample. The spectral emissivity at the pyrometer wave length was estimated from the spectral index of refraction. Using a spectral index value of 1.5, the spectral emissivity was estimated to be 0.92 by assuming reflection from two surfaces of the droplet. The apparent temperatures were corrected for the spectral emissivity. The temperature of the levitated sample was controlled via the incident laser beam heating, which was electronically controlled in the range of 30–300 W. The levitated sample could be quenched by instantly blocking the laser beam with a shutter.

After levitation melting and cooling, the samples were recovered, weighed, and examined at up to 60× using a stereo optical microscope. Selected samples were prepared for examination by scanning electron microscope (SEM). We restrict this discussion to six droplets that crystallized spontaneously and ignore four of the droplets that contacted the nozzle. Their compositions were somewhat analogous to IIA chondrules (SiO_2-47.72 wt%, TiO_2-0.21 wt%, Al_2O_3-0.68 wt%, FeO-19.03 wt%, MnO-0.37 wt%, MgO-29.59 wt%, CaO-0.71 wt%, Na_2O-1.56 wt%, K_2O-0.22 wt%). The weights of the droplets ranged from 20–30 mg and crystallized with slow recalescence of over one to two minutes. The temperatures of spontaneous crystallization ranged from 1450–1538 K with an average temperature of 1483 K. Hewins et al. examined three of these spherules that were fine-textured like CC chondrules, but were not exactly equivalent in texture to the CC chondrules. This is probably because the droplet temperatures were generally not uniform in our experimental examinations, and because the compositions were not the same as CC chondrules. In any case, the properties of these spontaneously crystallized spherules of type IIA composition parallel and are analogous to CC chondrules. Since it is harder to nucleate pyroxene than olivine, droplets are likely to crystallize spontaneously at lower temperatures for compositions in which pyroxenes should be the major mineral formed. Thus, the average of 1483 K should be an approximate upper limit for spontaneous crystallization of CC chondrules, the last to form. In our calculations at 0.1 bar, the calculated average temperature of crystallization of CC chondrules was 1435 K. This appears to be relatively close to reality.

CONCLUSIONS

Our discussion supports the conclusion that our calculations lend strong support to the constrained equilibrium theory and suggest the possibility of other relatively small non-equilibrium phenomena. Our concepts constitute the first unified set of simple believable ideas that explains the complexity of the chemistries of chondrules and LL chondrites. We hope to perform similar calculations for other classes of chondrites (e.g., carbonaceous and enstatite chondrites) at different ranges of temperatures and pressures.

In the model for our calculations, we have assumed a constant pressure with a decrease in temperature. The temperatures of formation at 0.1 bar pressure range from 1547 K to 1435 K. The volume of the gas would thus decrease by about 7% at constant pressure. Our experience indicates that such a small change would have negligible influence on the chemistry if the 7% shift in density or pressure is assumed. This model is at one end of the range of possibilities for cooling the gas, in which the gas might cool by radiation. At the other end, the gas can cool adiabatically by the expected expansion of the nebula gas late in the formation of the sun. The initial pressure need not be 0.1 bar, but can be higher and closer to the sun at <1 AU. At the time of formation of chondrules, the pressure need not be too distant from 0.1 bar. We hope to be able to calculate condensation in such gaseous expansions, which should occur late in the formation of the sun at a time when the sun's gravitational pull decreases or increases too slowly because of some energetic explosions, and because the total influx of gases into the nebula is slowed since the average travel distance increases for more distant gases, leading to a decrease in pressure. This would ultimately reverse the influx, and the pressures and temperatures of the gas would decrease simultaneously more rapidly.

REFERENCES

Anders E. and Grevesse N. 1989. Abundances of the elements, meteoritic and solar. *Geochimica et Cosmochimica Acta* 53: 197–214.

Bell K. R., Cassen P. M., Klahr H. H., and Henning T. H. 1997. The structure and appearance of protostellar accretion disks: Limits on disk flaring. *The Astrophysical Journal* 486:372–387.

Blander M. 1953. The differential diffusion coefficients of rubidium chloride, potassium per chlorate and cesium chloride in aqueous solutions at 25 °C. Ph.D. thesis, Yale University, New Haven, Connecticut, USA.

Blander M. and Abdel-Gawad M. 1969. The origin of meteorites and the constrained equilibrium condensation theory. *Geochimica et Cosmochimica Acta* 33:701–116.

Blander M. and Katz J. L. 1967. Condensation of primordial dust. *Geochimica et Cosmochimica Acta* 31:1025–1034.

Blander M. and Pelton A. D. 1983. *Computer assisted analyses of the thermodynamic properties of slags in coal combustion systems*. Argonne, Illinois: National Technical Information Service.

Blander M. and Pelton A. D. 1984. Analyses and predictions of the thermodynamic properties of multicomponent silicates. Proceedings, Second International Symposium on Metallurgical Slags and Fluxes. pp. 295–304.

Blander M. and Pelton A. D. 1987. Thermodynamic analysis of binary liquid slags and prediction of ternary slag properties by modified quasi chemical equations. *Geochimica et Cosmochimica Acta* 51:85–95.

Blander M., Planner H. M., Keil K., Nelson L. S., and Richardson N. L. 1976. The origin of chondrules: Experimental investigation of metastable liquids in the system Mg_2SiO_4-SiO_2. *Geochimica et Cosmochimica Acta* 40:889–896.

Blander M., Unger L., Pelton A. D., and Eriksson G. 2001. Nucleation constraints lead to molten chondrule precursors in the early solar system. *Journal of Physical Chemistry* B105:11,823–11,827.

Chartrand P. and Pelton A. D. 1999. Modeling the charge compensation effect in silica-rich Na_2O-K_2O-Al_2O_3-SiO_2 melts. *Calphad* 23:219–230.

Degterov S. and Pelton A. D. 1996a. Critical evaluation and optimization of the thermodynamic properties and phase diagrams of the CrO-Cr_2O_3, CrO-Cr_2O_3-Al_2O_3, and CrO-Cr_2O_3-CaO Systems. *Journal of Phase Equilibria* 17:476–487.

Degterov S. and Pelton A. D. 1996b. Critical evaluation and optimization of the thermodynamic properties and phase diagrams of the CrO-Cr_2O_3-SiO_2 and CrO-Cr_2O_3-SiO_2-Al_2O_3 systems. *Journal of Phase Equilibria* 17:488–494.

Degterov S. and Pelton A. D. 1997. Critical evaluation and optimization of the CrO-Cr_2O_3-SiO_2-CaO system. *Metallurgical and Materials Transactions B* 28:235–42.

Degterov S. Jak J., Hayes P., and Pelton A. D. 2001. Experimental study of phase equilibria and thermodynamic optimization of the Fe-Zn-O system. *Metallurgical and Materials Transactions B* 32: 643–658.

Degterov S., Jung I. H., and Pelton A. D. 2002. Thermodynamic modeling of the FeO-Fe_2O_3-MgO-SiO_2 System. *Journal of the American Ceramic Society* 85:2903–2910.

Eriksson G. 1975. Thermodynamic studies of high-temperature equilibrium. XII. Solgasmix, a computer program for calculation of equilibrium compositions in multiphase systems. *Chemica Scripta* 8:100–103.

Eriksson, G. and Pelton A. D. 1993. Critical evaluation and optimization of the thermodynamic properties and phase diagrams of the CaO-Al_2O_3, Al_2O_3-SiO_2, and CaO-Al_2O_3-SiO_2 systems. *Metallurgical Transactions* 24B:807–816.

Eriksson G., Wu P., and Pelton A. D. 1993a. Critical evaluation and optimization of the thermodynamic properties and phase diagrams of the MgO-Al_2O_3, MnO_2-Al_2O_3, FeO-Al_2O_3, Na_2O-Al_2O_3, and K_2O-Al_2O_3 systems. *Calphad* 17:189–206.

Eriksson G., Wu P., and Pelton A. D. 1993b. Critical evaluation and optimization of the thermodynamic properties and phase diagrams of the MnO-TiO_2, MgO-TiO_2, FeO-TiO_2, $T1_2O_3$-TiO_2, Na_2O-TiO_2, and K_2O-TiO_2 systems. *Metallurgical and Materials Transactions B* 24:795–805.

Eriksson G., Wu P., Blander M., and Pelton A. D. 1994. Critical evaluation and optimization of the thermodynamic properties and phase diagrams of the MnO-SiO_2 and CaO-SiO_2 systems. *Canadian Metallurgical Quarterly* 33:13–22.

Frurip D. J., and Bauer S. 1977. Homogeneous nucleation in metal vapors. 3. Temperature dependence of the critical supersaturation ratio for iron, lead, and bismuth. *Journal of Physical Chemistry* 81:1001–1006.

Gooding J. L. and Keil K. 1981. Relative abundances of chondrule primary textural types in ordinary chondrites and their bearing on conditions of chondrule formation. *Meteoritics* 16:17–43.

Grossman J. N., Alexander C. M. O'D., Wang J., and Brearley A. J. 2000. Bleached chondrules: Evidence for widespread aqueous processes on the parent asteroids of ordinary chondrites. *Meteoritics & Planetary Science* 35:467–486.

Hillert M., Janson B., and Sundman B. 1988. Application of the compound-energy model to oxide systems. *Zeitschrift für Metallkunde* 79:81–87.

Jones R. H. 1990. Petrology and mineralogy of type II FeO rich chondrules in Semarkona (LL3.0): Origin by closed-system fractional crystallization with evidence for supercooling. *Geochimica et Cosmochimica Acta* 54:1785–1802.

Jones R. H. 1994. Petrology of FeO poor porphyritic pyroxene chondrules in the Semarkona chondrite. *Geochimica et Cosmochimica Acta* 58:5325–5340.

Jones R. H. 1996a. Relict grains in chondrules: Evidence for chondrule recycling. In *Chondrules and the protoplanetary disk*, edited by Hewins R. H., Jones R. H., and Scott E. R. D. Cambridge: Cambridge University Press. pp. 197–204.

Jones R. H. 1996b. Fe-rich porphyritic pyroxene chondrules in unequilibrated ordinary chondrite. *Geochimica et Cosmochimica Acta* 60:3115–3138.

Jones R. H. and Scott E. R. D. 1989. Petrology and thermal history of type IA chondrules in the Semarkona (LL3.0) chondrite. Proceedings, 19th Lunar and Planetary Science Conference. pp. 523–536.

McCoy T. J., Scott E. R. D., Jones R. H., Keil K., and Taylor G. J. 1991. Composition of chondrule silicates in LL3-5 chondrites and implications for their nebular history and parent body metamorphism. *Geochimica et Cosmochimica Acta* 55:601–619.

Pelton A. D. 1999. Thermodynamic calculation of gas solubilities in oxide melts and glasses. *Glastechnische Berichte* 72:214–226.

Pelton A. D., Bale C. W., Thompson W. T., and Eriksson G. 2003. FactSage-an integrated thermodynamic databank system for inorganic applications. Last accessed from http://www.factsage.com on January 5, 2005.

Pelton A. D. and Blander M. 1984. Computer-assisted analysis of the thermodynamic properties and phase diagram of slags. Proceedings, AIME Symposium on Metallurgical Slags and Fluxes. pp. 281–294.

Pelton A. D. and Blander M. 1986. Thermodynamic analysis of ordered liquid solutions by a modified quasi chemical approach–Application to silicate slags. *Metallurgical and Materials Transactions B* 17:805–815.

Pelton A. D., Eriksson G., and Romero-Serrano J. A. 1993. Calculation of sulphide capacities of multicomponent slags. *Metallurgical and Materials Transactions B* 24:817–825.

Pelton A.D. and Chartrand P. 2001. The modified quasi chemical model II–Multicomponent solutions. *Metallurgical and Materials Transactions A* 32:1355–1360.

Reddy R. G. and Blander M. 1987. Modeling of sulphide capacities of silicate melts. *Metallurgical and Materials Transactions B* 8: 591–596.

Reddy R. G. and Blander M. 1989. Sulphide capacity of MnO-SiO_2 and other systems. *Metallurgical Transactions* 20B:137–140.

Wu P., Eriksson G., and Pelton A. D. 1993a. Critical evaluation and optimization of the thermodynamic properties and phase diagrams of the Na_2O-SiO_2 and K_2O-SiO_2 systems. *Journal of the American Ceramic Society* 76:2059–2064.

Wu P., Eriksson G., and Pelton A. D. 1993b. Critical evaluation and optimization of the thermodynamic properties and phase diagrams of the CaO-FeO, CaO-MgO, CaO-MnO, FeO-MgO, FeO-MnO, and MgO-MnO systems. *Journal of the American Ceramic Society* 76:2065–2075.

APPENDIX

The rapid crystallization of the liquid silicate droplets introduces a secondary non-equilibrium factor in the formation of chondrules. If gaseous materials enter or exit a droplet, the rapidly formed compact groups of crystals would hinder the process in the very brief moments of most of the crystallization. That is, rapid crystallization can block the transfer of materials between the gas phase and the chondrules during solidification, thereby resulting in a final chondrule composition closer to that of the initial precursor droplet. As discussed earlier, this effect would be most pronounced in the case of IA chondrules, where crystallization is expected to be most rapid. In fact, the measured IA composition actually agrees more closely with the calculated composition of the precursor droplets (Table 3) than with the composition calculated assuming transfer with the gas phase (Table 2). With FeO-rich IIA chondrules, the olivine formed is less alkaline than that of IA, and is likely to attempt to volatilize less silica and condense less MgO than type IA. An opposite possibility occurs when pyroxene crystallizes in chondrule types IAB, IB, IIAB, and IIB, SiO_2 tends to be taken in, and some MgO tends to volatilize if the crystallization is slow enough.

There is another, secondary non-equilibrium effect that may occur in all chondrules. With liquids deeply subcooled, the activities of more than one phase can be large enough to crystallize both liquids, for example, olivine and pyroxene, simultaneously. Hence, both solid phases can nucleate and grow, but one may form faster than the other, such that its final mass relative to the other phase will be greater than that calculated, assuming complete equilibrium. In experiments with molten droplets of different MgO-SiO_2 compositions (Blander et al. 1976) formed by SiO_2 volatilization from molten enstatite, only forsterite (an olivine) crystallized and no enstatite (a pyroxene) crystallized. This led to a mixture of forsterite with about 70 wt% of silica. In recent laboratory experiments with type IA and IIA compositions, pyroxene did form when the compositions contained some FeO. The fact that the pyroxene structure is more complex than olivine suggests that the kinetics of crystallization and growth of pyroxene is slower than that of olivine and, in subcooled metastable liquids, olivine could over-crystallize, that is, form more olivine and less pyroxene than would be present at equilibrium. A supercooled droplet crystallizes very rapidly once solid nucleation occurs. As discussed earlier, the latent heat of crystallization is evolved rapidly and heats the droplet temporarily to a temperature well above the ambient temperature. The droplet then rapidly cools back to the ambient temperature. Crystallization occurs throughout the heating and cooling cycle. At the higher temperatures, larger amounts of olivine and liquid silica are formed because reaction [1] is thermodynamically displaced to the left at higher temperatures. Under equilibrium conditions, this excess olivine and silica would then backreact as the droplets cooled back to the ambient temperature to form pyroxene by reaction [1] occurring to the right. However, since the cooling is very rapid, equilibrium is not attained. As a result, the amount of silica in the liquid (mesostases) in the final solidified chondrules will be greater than that calculated for thermodynamic equilibrium. That is, the solidification follows a classical path of non-equilibrium peritectic solidification. Since the total mass of the mesostases is small, a small excess of silica will result in a large observed shift in the composition of the mesostases. Rhian Jones (Jones 1994, 1996a, 1996b) has astutely observed that olivine crystallizes before and/or accompanies pyroxene crystallization in most chondrule types. We believe that this lends support to our hypotheses.